Application of Synthetic Aperture Focusing Technique for inspection of plate-like structures using EMAT generated Lamb waves

Yordan Mirchev[1,*], *Krasimir* Staykov[2], and *Damyan* Ganchev[2]

[1] Institute of Mechanics, Bulgarian Academy of Sciences, Sofia, Bulgaria
[2] Technical University of Sofia, Sofia, Bulgaria

Abstract. The main challenge for guided wave inspection is exact defect characterization and sizing. EMAT generated Lamb waves usually have low signal-to-noise ratio which reduces the defect detection, characterization and sizing capabilities. That's why in most cases the method is used only as a screening tool. The Synthetic Aperture Focusing Technique is a process that increases the signal-to-noise ratio by numerically focusing the acoustic fields. In this paper the application of SAFT is tested over EMAT generated Lamb waves. The improvement of lateral resolution and signal-to-noise ratio is evaluated. Results are presented as a comparison between standard B-scan and SAFT processed data.

1 Introduction

Application of ultrasonic guided waves in non-destructive testing is growing rapidly for a variety of reasons. Quite often this is the only way to solve a problem because of limited access to a structure and their ability to inspect large area from a single position [1]. Recently, a lot of industrial solutions based on EMAT generated guided waves have been developed. EMAT is contactless technology, which makes it very well suited for automated inspection. Also EMAT can inspect through coatings and are not affected by pollutants, oxidation, or roughness. The most common and simplest configurations for generation of guided waves in plates and pipes are the so-called meander coil EMAT. A meander coil in conjunction with a normal magnetic field causes a series of alternating tractions parallel to the surface of the sample. As a result, guided waves, with a wavelength equal to double the spacing between the wires, are excited [2]. This configuration has very good mode selectivity due to its meander-coil design and tone-burst excitation. The technique can cover shorter distances (0.1-3 m), compared to long range UT and can be used for detection of corrosion, cracks and discontinuities on exposed tubes, gas lines, oil pipelines and storage tanks. It typically works with frequencies ranging from 100 kHz to 1 MHz and has up to 10 times better resolution than long range UT systems with minimal or no dead zone.

* Corresponding author: mirchev@imbm.bas.bg

The equipment usually includes a hand-held scanner which provides axial and circumferential scanning for inspection of pipes and plates using guided waves. This allows real time images (B-scans) to be generated [3].

The main challenge in guided wave inspection is the exact defect characterization and sizing. That's why in most cases the method is used only as a screening tool. One of the signal processing techniques used in conventional ultrasonic testing to improve understanding of detected signals and increase defect sizing potential is Synthetic Aperture Focusing Technique (SAFT) [4].

The SAFT analysis is an imaging process that increases the signal-to-noise ratio and improves lateral resolution by numerically focusing the acoustic fields. More recently, this imaging technique has been applied to imaging defects in plates using guided waves generated using piezoelectric transducers [5-6].

In this paper an offline post-processing SAFT technique is described which uses the complete B-scan data recorded from hand-held scanning of steel plates using EMAT generated Lamb waves.

2. Data post-processing algorithm

The movement of the EMAT transducer simulates a multi element synthetic aperture, where every element transmits and receives simultaneously. Schematic representation of the synthetic aperture is presented on fig. 1. For each position of the transducer *n* at regular intervals raw A-scans are recorded and no time correction is applied at that time.

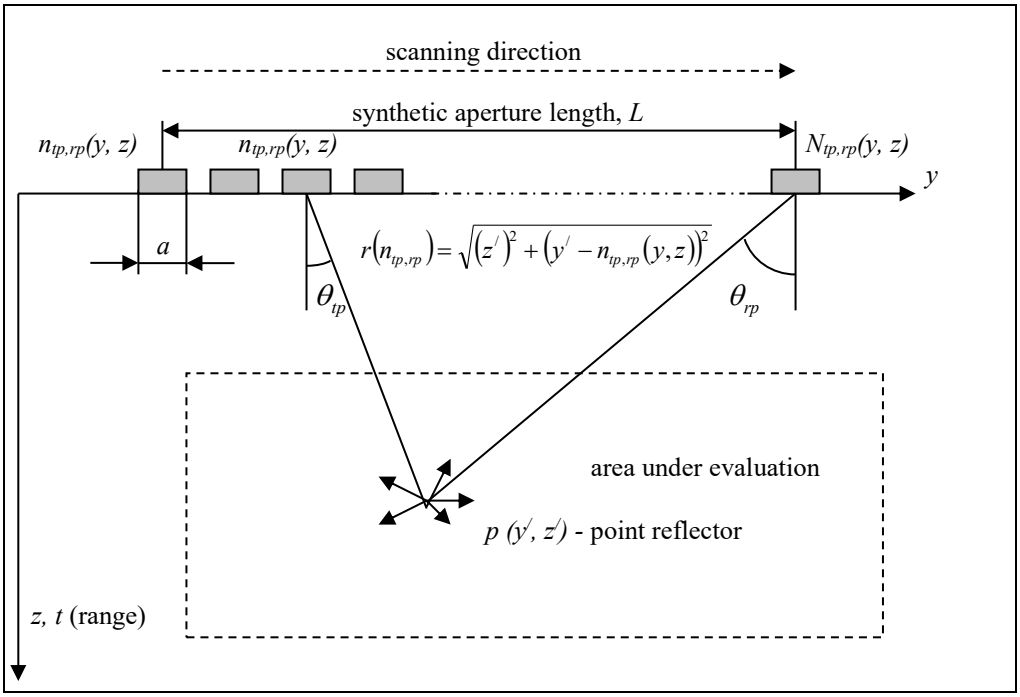

Fig. 1. Schematic representation of the synthetic aperture obtained by mechanical scanning

Flow chart of the data post-processing algorithm is presented on fig. 2.

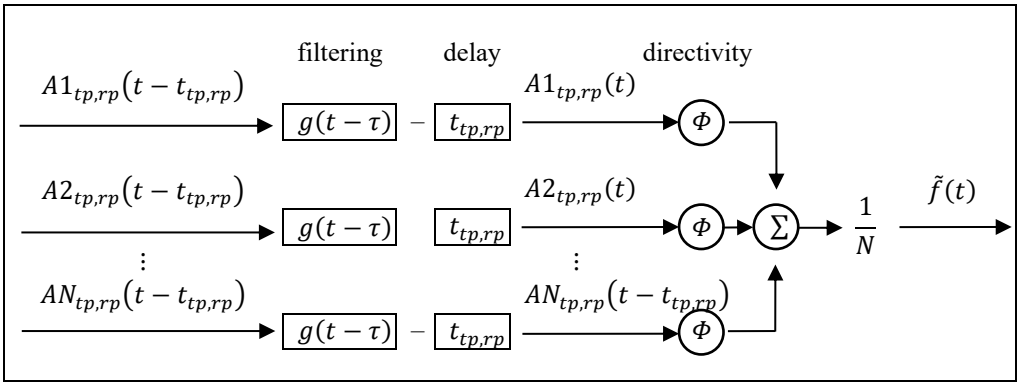

Fig. 2. Post-processing algorithm

The information signals $An_{tp,rp}(t-t_{tp,rp})$ are represented in a matrix giving an unprocessed B-scan image. Each signal is processed by a bell shaped correlation function $g(t-\tau)$ using the following equation:

$$An_{tp,rp} = A_0 e^{i\omega_0(t-t_{tp,rp})-\beta^2\omega_0^2(t-t_{tp,rp})^2}, \tag{1}$$

where A_0 is the maximum value of the transmitted impulse (in all cases in the present work $A_0 = 1$), e – Euler's number, $\omega_0 = 2\pi f_0$ – nominal angular frequency, f_0 – nominal linear frequency, t – time scale or range, $\beta = \frac{0.265}{m}$ – pulse shape and length coefficient, m – number of oscillations in the pulse at -6 dB level, $t_{tp,rp} = \frac{d_{tp,rp}}{C}$ – pulse time-of-flight for distance $d_{tp,rp}$ and velocity of ultrasonic waves in the test environment C, j – imaginary unit, k – wave number.

To reduce the noise in the received signal, a short-time Fourier transform is used. It is given by the following equation:

$$xn_{tp,rp}(\tau,\omega) = \int_{-\infty}^{\infty} An_{tp,rp}(t)gn_{tp,rp}(t-\tau)e^{-j\omega t}dt. \tag{2}$$

The filtered signal is represented by dependence (3) for the nominal angular frequency ω_0 of the probe. The Fourier spectrum of the processed signal is calculated with the following equation:

$$Fn_{tp,rp}(\omega) = \int_{-\infty}^{\infty} xn_{tp,rp}(\tau,\omega)d\tau. \tag{3}$$

Compensation of the delay time in the signal's spectrum for every individual position of the probe is given with the following dependence:

$$Gn_{tp,rp}(\omega) = Fn_{tp,rp}(\omega)e^{jk(\omega)(d_{tp,rp}-z')}, \tag{4}$$

where $d_{tp,rp}$ is the distance traveled by the wave from the transmitter to the reflecting point $p(z',y')$ and back to the receiver. z' - is the distance along the Z axis perpendicular to the scanning axis Y.

For the SAFT algorithm the distance $d_{tp,rp}$ is calculated as follows [7]:

$$d_{tp,rp} = 2r\left(n_{tp,rp}\right) = 2\sqrt{(z')^2 + \left(y' - n_{tp,rp}(y,z)\right)^2}, \tag{5}$$

where z' and y' – the coordinates of the point reflector, tp and rp – refer to the operation of the probe as emitter and receiver for the point reflector p in the area under consideration, n – position of the probe during mechanical scanning.

The response spectrum is calculated after the time delay is compensated. The directional characteristics of the ultrasonic probe and the amplitude drop due to beam divergence are also taken into account. This is achieved with the following dependence:

$$Hn_{tp,rp}(\omega) = \frac{\Phi n_{tp,rp} G n_{tp,rp}(\omega)}{\sqrt{r\left(n_{tp}\right) r\left(n_{rp}\right)}}, \tag{6}$$

$$\Phi n_{tp,rp} = \frac{\sin\left(\frac{a}{2} k \sin\left(\Theta_{tp,rp}\right)\right)}{\frac{a}{2} k \sin\left(\Theta_{tp,rp}\right)}, \tag{7}$$

where a is the length of the probe, $\Theta_{tp,rp}$ – the angle between the Z axis of the probe and the point reflector $\mathrm{p(z', y')}$ given on fig. 1, k – wave number.

From the dependence (6) signals $Xn_{tp,rp}(t)$ are obtained by a reverse Fourier transformation for each point of the area under evaluation using the following equation:

$$Xn_{tp,rp}(t) = \int_{-\infty}^{\infty} Hn_{tp,rp}(\omega) e^{j\omega t} d\omega. \tag{8}$$

The final transformed B-scan is calculated using:

$$h(z,y) = \sum_{n} Xn_{tp,rp}\left(\frac{d_{tp,rp}}{C}\right). \tag{9}$$

3. Used equipment, samples and experimental procedure

Experiment are conducted to evaluate the suitability of proposed SAFT post-processing for application in inspection of plate-like structures using EMAT generated Lamb waves. During the experiments an Innerspec Powerbox H ultrasonic instrument with permanent magnet sensor and temate® MRUT hand-held scanner is used. The sensor consists of "XXL" magnets and corresponding "hourglass" coils [3]. Evaluated samples are steel plates (grade S235JR according to EN 10025:2005) having dimensions 1000x200 mm and thickness of 4 mm. In the samples a through holes are drilled having diameter d = 10 mm, 15 mm and 20 mm. For the experimental work A0 Lamb wave mode at frequency 405 kHz is generated using meander coil with period 6.35 mm and 5 cycle excitation pulse. The EMAT transducer length is 50 mm, and the selected aperture length is 100mm. The samples are scanned according to the scheme shown on fig. 3. The distance between the EMAT and the through hole defect is 300 mm. During the scanning B-scans are recorded composed of A-scans at 1 mm steps in lateral direction. The sampling frequency was set to 10 MHz.

All B-scans are then post-processed offline using SAFT algorithm described above.

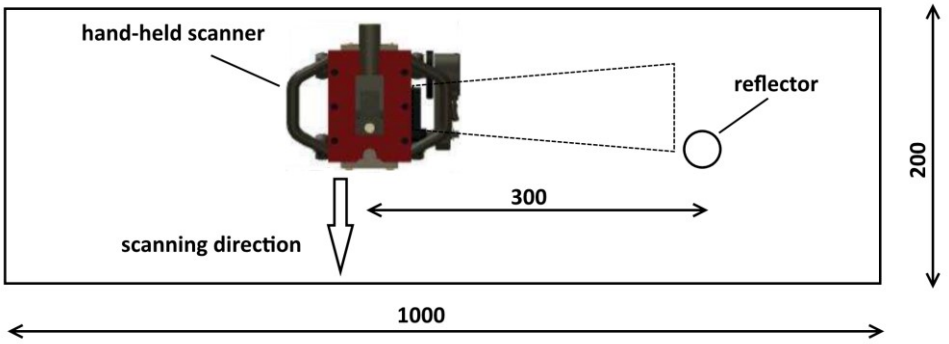

Fig. 3. Scheme showing the through hole reflector and the scanner during the experiments.

4. Results and discussion

On fig. 4 are presented B-scans from the experiments for different diameter reflectors and their corresponding SAFT processed images (eq. 9). On the B-scans are shown RF signals reflected from through holes having diameter d = 20 mm, 15 mm and 10 mm. Scanning direction is aligned with the Y-axis and the position changes from 0 to 100 mm. The Z-axis corresponds to the direction of sound propagation and is presented from 270 mm to 350 mm in front of the transducer position. The amplitude of the signal is encoded in gray scale.

After processing the initial B-scans with the proposed SAFT algorithm the width of the reflected ultrasonic beam in the scanning direction Y-axis is reduced. This can clearly be seen on fig. 4b, 4d and 4f. Considerable noise reduction can also be seen. This leads to better spatial resolution in the scanning direction.

In order to evaluate the ultrasonic beam width data is extracted from the recorded B-Scans at distance Z = 300 mm. This corresponds to the center line of the trough holes. The resulting graphs in the form of normalized amplitude at different lateral positions of the scanner are presented on fig. 5.

Data from scanning a 10 mm diameter through hole, presented on fig. 5c, shows that the ultrasonic beam width at -6dB is equal to 44 mm. After post-processing with the proposed algorithm the beam width is reduced to 30 mm. The improvement of spatial resolution in the scanning direction would be around 30%. Furthermore an improvement of signal-to-noise ratio around 18 dB was also observed. Similar results are observed from the scanning of other samples.

The results show the ability of SAFT to increase the inspection range and respectively the sensitivity of meander coil EMAT equipment. This post-processing additionally allows more precise characterization of discontinuities in plate-like structures tested using guided waves.

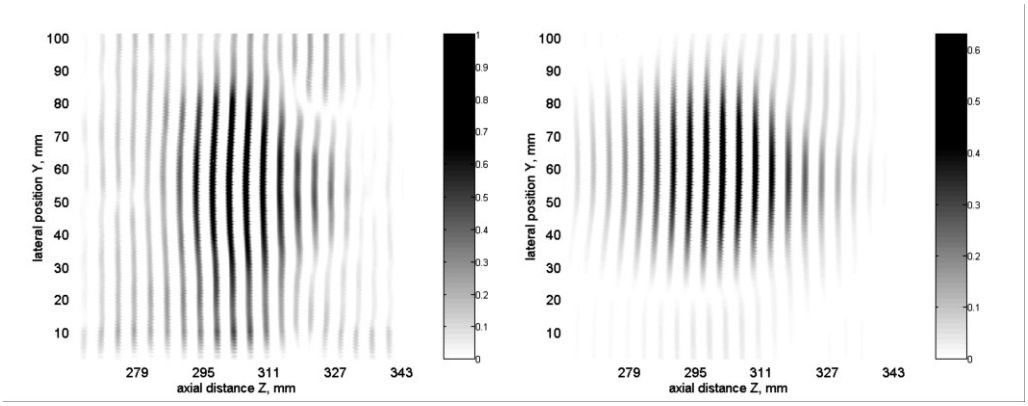

a) B-scan, *d = 20 mm* b) SAFT, *d = 20 mm*

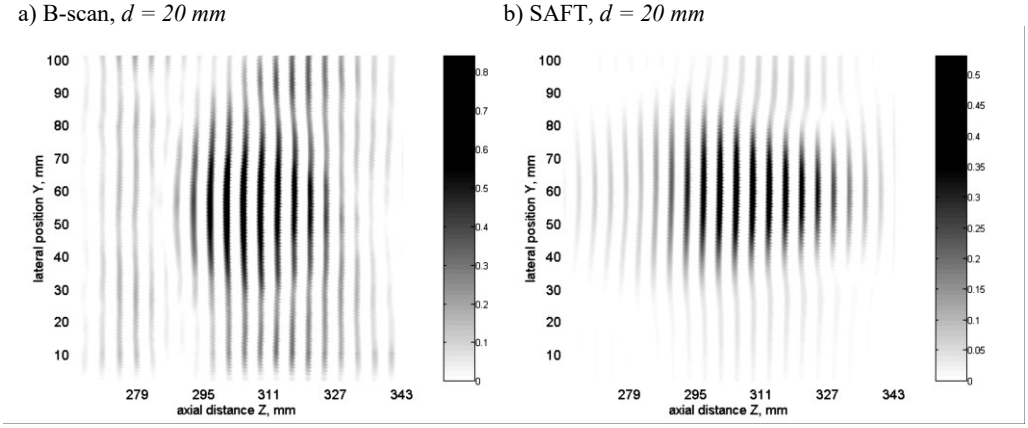

c) B-scan, *d = 15 mm* d) SAFT, *d = 15 mm*

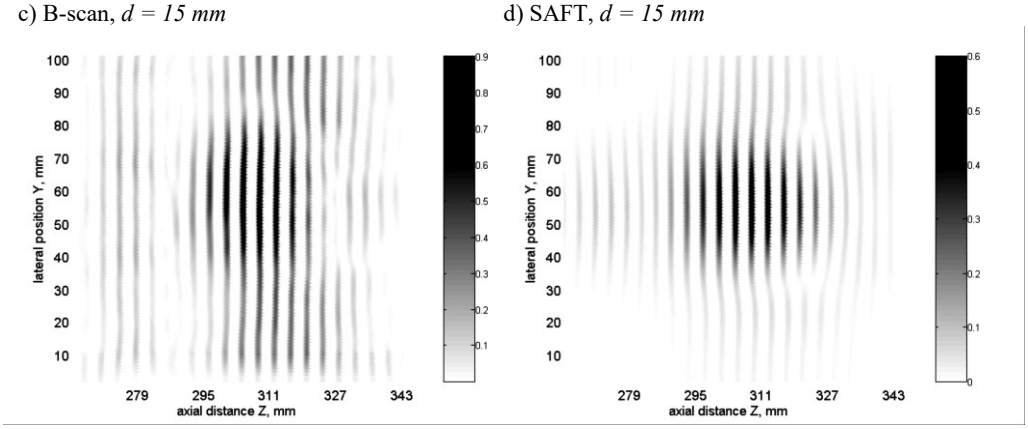

e) B-scan, *d = 10 mm* f) SAFT, *d = 10 mm*

Fig. 4. B-scan images from the ultrasonic testing and their corresponding SAFT processed images

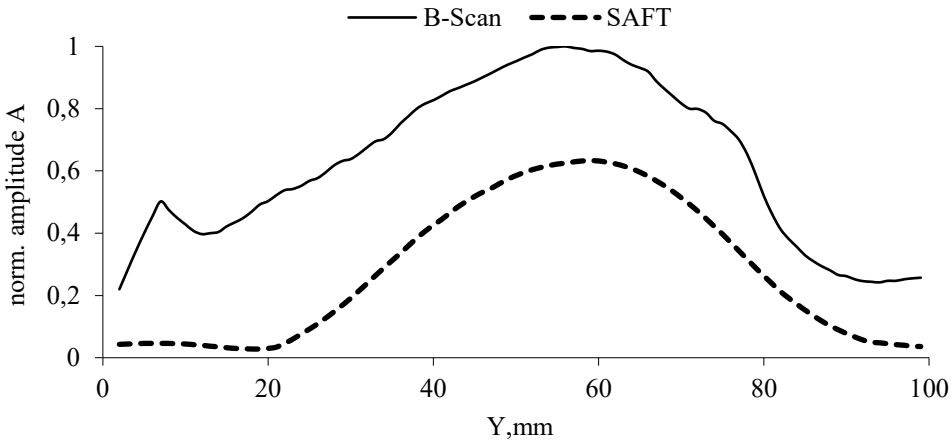

a) d = 20 mm

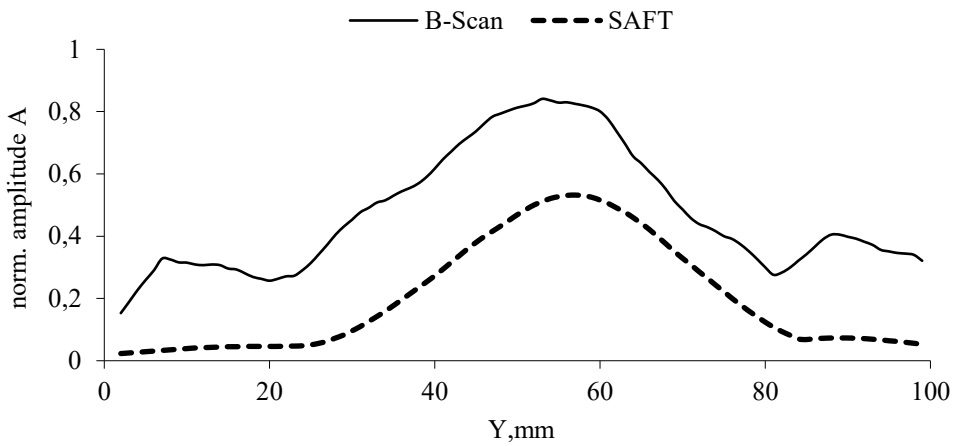

b) d = 15 mm

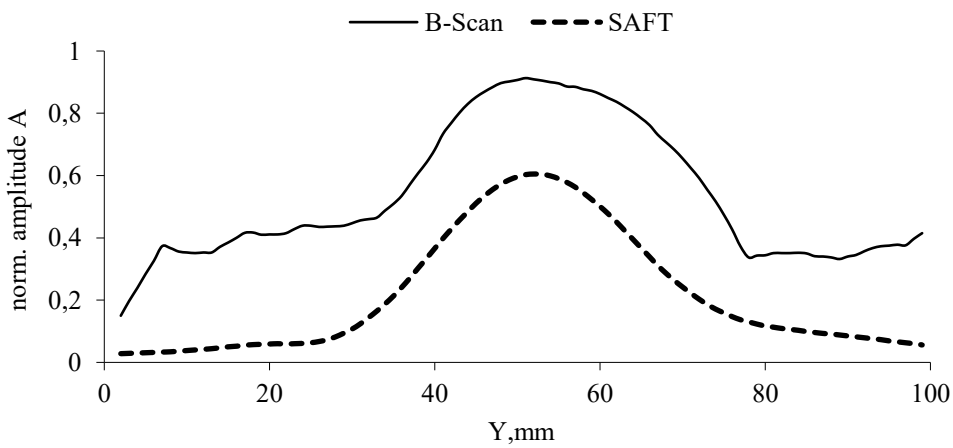

c) d = 10 mm

Fig. 5. Width of the ultrasonic beam at distance Z = 300 mm

5. Conclusion

The proposed algorithm for post-processing of ultrasonic signals received from EMAT generated Lamb waves is based on SAFT. The experimental results show around 30% improvement of the lateral resolution at -6 dB level. Improvement of the signal-to-noise ratio (more than 16 dB) is also observed which is of great importance in EMAT ultrasonic testing known with its low SNR. One advantage is that the focusing possibility is independent on the length of the sound path. Those results show the ability of proposed algorithm to improve defect sizing and characterization capabilities of conventional EMAT generated Lamb waves inspection techniques. The proposed off-line processing technique can be embedded into new inspection equipment as a real-time version that will enhance the defect detection and evaluation potential.

6. References

1. J. L. Rose, *Proc. SPIE* **7983**, 798302 (2011)
2. R. Ribichini, *Modelling of electromagnetic acoustic transducers*, PhD thesis, Imperial College London, London (2011)
3. Innerspec Technologies, Inc., http://innerspec.com/en/
4. J. Pitkänen, *ECNDT 2006*, Poster 211 (2006)
5. J. Davies, F. Simonetti, M. Lowe, P. Cawley, *ECNDT 2006*, Tu.4.1.3 (2006)
6. R. Sicard, A. Chahbaz. J. Goyette, IEEE Trans. Ultrason. Ferroelec. Freq. Cont. **51**, 1287-1297 (2004)
7. C. Holmes, B. Drinkwater, P. Wilcox, NDT & E Intern. **38**, 8, 701-711 (2005)